Towards accurate dielectric property retrieval of biological tissues for blood glucose monitoring

Yilmaz, T; Foster, R; Hao, Y

T. Yilmaz, R. Foster and Y. Hao, “Towards Accurate Dielectric Property Retrieval of Biological Tissues for Blood Glucose Monitoring”, *IEEE Trans. Microw. Theory Techn.*, vol. 62, no. 12, pp. 3193-3204, Dec. 2014.

This post-acceptance version of the paper is essentially complete, but may differ from the official copy of record, which can be found at the following web location (subscription required to access full paper): http://dx.doi.org/10/1109/TMTT.2014.2365019.

Towards Accurate Dielectric Property Retrieval of Biological Tissues for Blood Glucose Monitoring

Tuba Yilmaz, Robert Foster, *Member, IEEE*, and Yang Hao, *Fellow, IEEE*

***Abstract*—An analytical formulation for relative dielectric constant retrieval is reconstructed to establish a relationship between the response of a spiral microstrip resonator and effective relative dielectric constant of a lossy superstrate, such as biological tissue. To do so, an analytical equation is modified by constructing functions for the two unknowns, filling factor A and the effective length l_{eff} of the resonator. This is done by simulating the resonator with digital phantoms of varying permittivity. The values of A and l_{eff} are determined for each phantom from the resulting S-parameter response, using Particle Swarm Optimization. Multiple non-linear regression is applied to produce equations for A and l_{eff}, expressed as a function of frequency and the phantom's relative dielectric constant. These equations are combined to form a new non-linear analytical equation, which is then solved using the Newton-Raphson iterative method, for both simulations and measurements of physical phantoms. To verify the reconstructed dielectric constant, the dielectric properties of the physical phantoms are determined with a commercial high temperature open-ended coaxial probe. The dielectric properties are reconstructed by the described method, with less than 3.67% error with respect to the measurements.**

***Index Terms*—dielectric property retrieval, high-permittivity materials, high-loss materials, non-invasive glucose monitoring, spiral resonator.**

I. Introduction

It is now recognized that the demographic changes occurring in society, particularly the aging of the increasing global population, have profound implications and create many challenges in the provision of health care. Utilization of technology can greatly aid in meeting these challenges, including the development of ubiquitous health care. A key component in realizing ubiquitous health care (that is, health care provision everywhere—home, hospital, shop, street) is the development of wireless physiological sensors and associated systems, usually linked into wearable wireless body area networks (WBANs). Such monitoring covers various 'vital signs', including the heart-beat waveform (ECGs, or electrocardiographs), blood pressure, pulse rate, breathing (respiration) rate, oxygen saturation (concentration of oxygen in the blood) and blood glucose level. A recent survey of work in this area is given in [1], whilst a review of the requirements of WBANs is provided in [2].

Blood glucose monitoring is of particular concern due to the increase in the number of diabetes patients, in part due to the aging of the population, in part due to the rise of obesity. Standard methods require the periodic sampling of blood, with an enzyme-based detection method employed to determine the actual blood glucose level (BGL). More recently, attention has turned to non-invasive or minimally-invasive methods (usually requiring a bio-sensor), in order to realize the continuous monitoring of BGL. A review of the current state-of-the-art in continuous glucose monitoring, including both minimally-invasive and non-invasive techniques, is given in [3].

Non-invasive methods avoid the need for penetration of the skin, removing any risk of infection, as well as avoiding some psychological barriers from some patients. The main (non-optical) method investigated to date is impedance spectroscopy, whereby the skin surface impedance is measured and observed changes are related to alterations in BGL. This results in part from the fact that the dielectric properties of erythrocyte (red blood cell) membranes are affected by the concentration of glucose, affecting in turn the electrolyte balance of skin and subcutaneous tissue. The amount of such change depends on the operation frequency [4], [5]. However, one drawback is that other physiological processes also affect the response of the RF device, including such things as sweat levels, changes in posture, and temperature levels. This makes unambiguous determination of BGL challenging.

The utilization of RF techniques for BGL monitoring has been investigated in the past. These studies typically observe the changes in the S-parameter response of an antenna or resonator, which occurs due to the changes in dielectric properties of the propagation medium, the biological tissue. A change in BGL leads to a change in the effective dielectric constant of the body, which can thus be detected, in principle, from a change in the resonant frequency determined by the antenna or resonator measurement. Work reported in the literature in this area includes both quantifying the effect of glucose on the dielectric properties and proposing antennas or resonators for measurement of such changes. In [6], an open-ended coaxial probe was used to determine the dielectric properties of blood for varying amounts of glucose in a controlled experiment. A wide-band monopole antenna was presented in [7], [8] for non-invasive BGL monitoring. In [9], a cavity resonator approach was taken and dielectric properties of blood characterized between 10 GHz and 20 GHz, for different glucose concentrations. Finally, in [10], a spiral resonator was employed (see Section II). Another spiral resonator was presented in [11], which used a multi-layer digital phantom of different tissues, with the tissue properties modeled with the second-order Debye equation. The use of a microstrip resonator was recently described [12] for an *in vitro* study

Manuscript received April 14, 2014 and revised July 11, 2014.

The authors are with the School of Electronic Engineering and Computer Science, Queen Mary College, University of London, London, E1 4NS. Email: y.hao@qmul.ac.uk

of blood with controlled amounts of glucose added. However, this work did not consider *in vivo* non-invasive applications, or use a spiral resonator.

The work presented in the following continues to explore the capabilities and issues relating to this technique. In particular, we focus on extracting the 'superstrate' permittivity (the phantom permittivity, or equivalent homogeneous body permittivity) from the resonator response, via the effective permittivity. The effective permittivity may be determined fairly easily through known techniques, but the determination of the phantom permittivity requires the adoption of a suitable model. The main contribution of this paper is the application of optimization and non-linear regression methods to determine relationship between the permittivity of a (lossy) superstrate and the resonant frequency of the loaded microstrip spiral resonator. This is a complementary approach to the theoretical or empirical methods often used, and can be applied more generally to other resonators and scenarios. Whilst the application of blood glucose monitoring provides the motivation for this work, and the general framework for the phantom preparation, we are not concerned with detecting realistic levels of sugar here. The glucose-dependent properties are outside the scope of this paper, but are under investigation by the authors. The sensitivity requirements for detection of realistic glucose levels have recently been discussed in [13]. It is also noted that the reported work applies to the dielectric characterization of non-biological materials with a spiral resonator, as well as the stated application of blood glucose monitoring.

This paper is organized as follows: the next section provides some background on microstrip resonators for dielectric property measurements, with an emphasis on biological applications. It also briefly reviews the Particle Swarm Optimization (PSO) method, utilized in this work due to its ease of implementation. The design of the resonator is described in Section III-A, with the experimental design described in Section III-B. The improved phantom permittivity retrieval method is described in Section III-C. Results are presented and discussed in Section IV, including further investigations into potential sources of error. Finally, conclusions are drawn in Section V.

II. Background

Microstrip resonators are lengths of microstrip transmission line that support standing waves at particular frequencies. The simplest is a straight section of microstrip [14]. Also common is the ring resonator, where the transmission line is formed into an annulus. Such resonators have been proposed for dielectric property measurements previously (e.g., [15]). Standard microstrip has air above the substrate. More complicated geometries are possible, utilizing additional dielectrics [16]. The analysis of the behavior of these lines is complicated by the multiple dielectrics. An effective medium approach is usually followed, where the geometry is replaced with one dielectric with material properties equivalent to the combination of the original materials. These are often determined using conformal mapping techniques that find equivalent filling fractions for each material [17]–[19], or the variational method (e.g., [20]). An alternative approach uses curve fitting to empirical or simulated data [16]. We use a variation of this approach in this work.

Spiral resonators are attractive for the relatively compact geometry and symmetry [10]; however, they introduce a further complexity into the analysis, namely the coupling between the adjacent lines, which modifies the effective permittivity of the equivalent homogeneous dielectric. Design equations are available for *co-planar stripline* spiral resonators [21], including with the presence of a superstrate, and depend on complete elliptic integrals of the first kind, evaluated numerically. Explicit expressions for the effective permittivity of a *microstrip* spiral structure have not been found in the literature, however, even for standard geometries with air above the substrate. The use of microstrip resonators for material characterization requires the presence of at least one superstrate, by definition. In the absence of analytical formulations, the behavior of a spiral resonator in this application must be investigated through numerical means. It is also noted that the (semi) analytical approaches, such as those taken in [15], [17]–[19], usually result in complex expressions that can only be evaluated numerically. Furthermore, the equations that *are* available for straight coupled microstrip lines (with an air superstrate) are extremely complicated, with multiple non-linear equations determined via curve-fitting of simulated data [16].

PSO, an evolutionary algorithm, was first introduced by Kennedy and Eberhart in 1998; since then, the algorithm has been applied to solve many different problems, including EM problems, such as optimization of free space and implantable antenna geometries for maximum bandwidth, gain, or to tune the antenna for a desired frequency of operation [22]–[27]. The algorithm finds an optimal solution to a problem from a pre-determined solution space by iteratively adjusting the trajectories of particles according to the personal best position of each particle and overall, global, best position of the swarm. The algorithm is powerful and simple and has a wide range of applications. In this paper, we used the algorithm to solve a two-dimensional problem, to relate the resonant frequency of the spiral resonator to the phantom permittivity. A review can be found in [28]. Its use in this work is due to its simplicity of implementation; other optimization techniques could be substituted.

In [10], a microstrip spiral resonator was proposed for non-invasive monitoring of BGL. Spiral microstrip resonators are attractive as they are low-cost, potentially conformal and relatively compact in size. In addition, the "*circular-like symmetry of the spiral makes it less sensitive to contact orientation...*" [10]. The resonator was tested on one subject and the transmission magnitude of the resonator was recorded as an initial step. The authors then modified the resonator and tested it on other subjects, demonstrating the ability to track glucose changes in each case, although the error could be as much as 19.5%. This work did not attempt to derive a closed-form relationship between resonant frequency and blood glucose. Instead, the data was 'calibrated' for each subject using principal component analysis, the results of which were used in multiple linear regression when comparing

against a commercial glucometer. However, the human body is a complex environment and there are many variables (such as temperature, sweat levels, and blood pressure) that can affect the effective permittivity of the tissues above the resonator. In addition, external effects, such as the applied pressure to the resonator, can change the response.

Although microstrip resonators are mainly utilized to retrieve the dielectric properties of low-loss and low-permittivity materials in the literature (e.g., [29], [30]), such resonators can also be utilized for dielectric property retrieval of biological tissues. The dielectric properties of biological tissues are mainly investigated with open-ended coaxial probes. Such probes provides ultra-wide band data; however, the data is usually lacking precision, the probes are costly, and the equipment is very bulky. Microstrip resonators are low-profile, can easily be integrated with remaining circuitry, can be miniaturized, and are cost-effective to produce. Thus, such resonators are well-suited for home or ambulatory applications.

The authors previously examined a microstrip spiral resonator with phantoms having different sugar levels, and the dielectric properties of the phantoms were recovered with an analytical equation [31]. However, this retrieval method required the measurement of two phantoms with known dielectric properties, as a means of calibration. The calibration method was rather inefficient and the retrieval error depended on the frequency shift during the calibration. In order to apply the RF methods for non-invasive BGL measurement, it is critical to establish a clear relationship between the (glucose-dependent) dielectric properties of biological tissues and the S-parameter response of the RF device. This paper reports the first step towards this goal, where an improved accuracy in the retrieval of the relative permittivity of a superstrate is demonstrated. In this paper: (1) the previous analytical equation is modified by utilizing simulation data, with the intention of eliminating the need for the calibration; and (2) to verify the validity of the method, the modified analytical equation is employed to reconstruct the relative dielectric constant of the phantoms proposed in [31]. The new technique is expected to perform better, since the simulation data provides *a priori* information based on the ideal case, whereas the pure measurement data used for calibration, when collected without much care (as may be the case with end-users), can lead to wrong retrieval values. The ultimate aim with this work is to produce a method of determining the *phantom* permittivity (not the *effective* permittivity) from the resonant frequency of the spiral resonator, taking into account various influences, to achieve a high accuracy and a fast and simple implementation (e.g., using a pre-calculated look-up table) for use in a wearable device (e.g., in a watch-type device or a 'digital plaster'). Introducing additional factors into the model is left for further work.

III. Design and Methodology

A. Design of the Spiral Resonator

The spiral resonator used in this work is shown in Fig. 1. It is a modified version of a design given in [10]. The original resonator was designed to be used as a complementary method

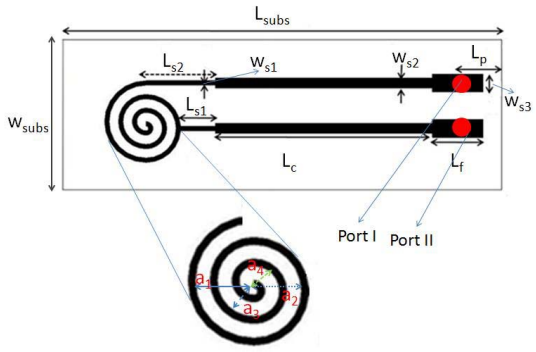

(a)

(b)

Fig. 1. Spiral microstrip resonator [10]: (a) structure; and (b) manufactured prototype. A ground plane covers the entire lower surface of the substrate (not shown).

TABLE I
Dimensions of the Spiral Microstrip Resonator (units: mm)

Parameter	Value	Parameter	Value	Parameter	Value
a_1	8.0	L_{subs}	95.00	w_{subs}	33.000
a_2	6.5	L_{s1}	7.51	w_{s1}	3.980
a_3	5.0	L_{s2}	15.00	w_{s2}	2.207
a_4	3.5	L_p	9.00	w_{s3}	1.000
a_5	2.0	L_f	11.00		
a_6	0.5	L_c	47.00		

to the traditional periodic lancet sampling, and required the user to press his thumb against the resonator for a short period of time. The design was re-implemented by the authors, using both FR-4 [32] and Taconic TLC(30) substrates [31]. The details of this modified design were not provided in the earlier papers [31], [32], so are given here.

The resonator was designed with CST Microwave Studio and printed on Taconic TLC(30) substrate, with a substrate thickness of 1.47 mm and $\epsilon_r = 3$. Dimensions are provided in Table I; the ground plane covered the reverse side of the substrate. One of the key benefits of a spiral resonator, as opposed to a ring or line resonator, is its compact size. The version discussed here is an early prototype and is, hence, still relatively large for the intended application of wearable continuous BGL monitoring; however, further size reduction is anticipated, even with the required integration of the necessary electronics. Although the design presented has two ports, we focused on the reflection coefficient for this paper, due to the relative sensitivity shown to permittivity changes. The simulated and measured performance of the unloaded resonator (i.e., with air above the substrate) is shown in Fig. 2.

In [32], the FR4 resonator was tested with liquid phantoms,

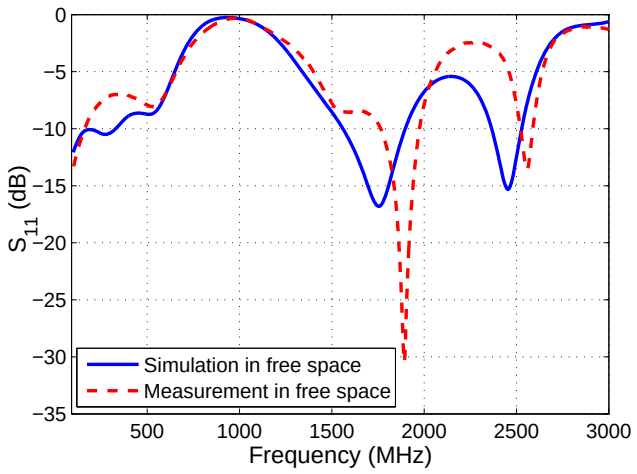

Fig. 2. Simulated and measured unloaded (free-space) performance of the spiral microstrip resonator, as determined by the impedance matching performance.

where the liquid phantoms were placed on top of the resonator in a plastic bag. The plastic bags introduced an air-gap between the resonator and the phantom; thus, the repeatability of the measurement results was low. The resonator fabricated on the Taconic TLC(30) substrate, reported in [31], was tested with semi-solid phantoms to investigate the repeatability of the measurements. The dielectric properties of the phantoms were then retrieved with an analytical method. However, the analytical method was ambiguous, due to the calibration procedure. 16 measurements with the resonator were considered for calculations in [31]. A further 44 measurements (60 in total) are included in the data-set for this paper, in which optimization techniques are utilized to improve the analytical formulation, with the intention of eliminating the need for the calibration procedure. We emphasize that our objective is not to determine the *effective* permittivity. We want a method of calculating the *phantom* permittivity from the measurement of a resonant frequency. No existing model relating the effective permittivity (measurable via the resonant frequency) to the superstrate permittivity has been found in the literature. This forces us to adopt a non-linear model with two coupled unknowns, described in the following sub-sections.

B. Experimental Methodology and Physical Phantom Preparation

Conceptually, the experimental methodology is simple. First, the physical phantoms are prepared; second, the dielectric properties of each phantom are measured across a wide frequency band using a vector network analyzer (Hewlett Packard 8720ES VNA) with an open-ended coaxial probe, as a reference for the resonator; finally, the resonator is used with each phantom, with S_{11} (magnitude and phase) measurements performed with the VNA. The phantoms used are termed gel-like; they are semi-solid and require protection from the atmosphere when not in use. This was achieved by covering them with plastic bags. It had been observed that the resonant frequency of the sensor is affected by the

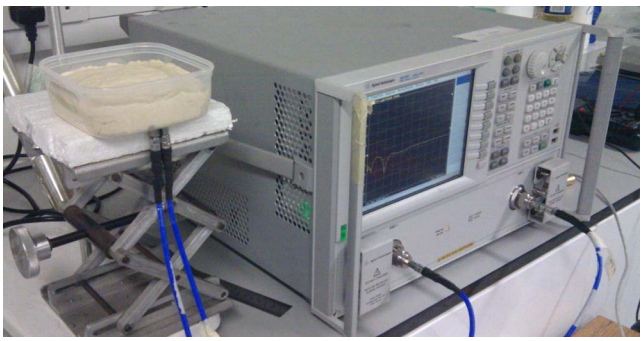

Fig. 3. S-parameter measurements with phantom material placed above the resonator [31].

thickness of the sample, the pressure applied to the resonator and the surface condition of the phantom [32]. Thus, the thicknesses and weights of the phantoms were kept constant. Ten measurements in total were performed per phantom, with the resonator mounted at the bottom of a container and each phantom placed just above the resonator. All measurements were performed at $21^{\circ}\mathrm{C}$.

The gel-like phantoms were created by preparing a set of liquid solutions, then mixing each with 170 g of flour. The liquids consisted of 100 g deionized water solutions with 5, 10, 15, 20, 25, and 30 percent sugar concentrations. Please note that the sugar concentrations are not representative of the blood glucose concentrations in humans. A recent study on the effect of realistic glucose-dependence of dielectric properties for blood tissue mimicking phantom (TMP) is revealed that the relative permittivity of the blood TMP decreases by 1 unit with maximum realistic change in glucose levels [13]. One unit change will approximately corresponds to increase in sugar content from 5% to 7%-7.5%. However, in this paper to prove the dielectric property retrieval concept higher sugar concentrations are considered. Water has the highest dielectric constant of these substances; the dielectric constant is reduced by adding the sugar and flour. The dielectric properties measured with the coaxial probe at resonance frequencies are given in Table II, and wide-band measurements are given in Fig. 4 (a)–(b) for permittivity and conductivity, respectively.

The resonator is a microstrip transmission line; it has resonances that are determined by the length of the line and the phase velocity in the effective medium formed by the substrate and the phantom under test. As these are non-magnetic, the phase velocity dependence is equivalent to a dependence on the effective dielectric constant of the medium. The resonances can be expressed by [29]:

$$f_n = \frac{nc_0}{l_{\text{eff}}\sqrt{\varepsilon_{\text{eff}}}} \tag{1a}$$

$$\implies \varepsilon_{\text{eff}} = \left(\frac{nc_0}{l_{\text{eff}} f_n}\right)^2 \tag{1b}$$

where n indicates the mode (number of the resonance, equal to two for the mode monitored in this work), c_0 is the speed of light, l_{eff} is the effective length of the microstrip line and ε_{eff} is the effective dielectric constant.

The effective dielectric constant can be related to the

dielectric constants of the substrate (ε_r) and phantom (ε_{p}) by:

$$\varepsilon_{\text{eff}} = A\varepsilon_r + B\varepsilon_{\text{p}} \tag{2a}$$
$$B = 1 - A \tag{2b}$$

where A is an unknown representing the proportion of the electric field propagating in the substrate, relative to that in the substrate and phantom (essentially a 'filling factor'). A is necessarily a function of frequency, the geometry of the resonator, the substrate and phantom permittivities, and the geometry of the phantom, making (2a) non-linear. The method of coupling to the resonator will also affect A and l_{eff}. However, the exact dependence on these factors is unknown. It is noted that ε_{p} can be considered the relative permittivity of a homogeneous phantom or the effective permittivity of a heterogeneous phantom, filling the half-space above the microstrip in either case. This is similar to approaches in the literature for standard microstrip (e.g., [16]), which assume air occupies the half space above the microstrip, meaning $\varepsilon_{\text{p}} = 1$. Furthermore, a sufficiently-thick material can be a good approximation to an infinite half space at a given frequency, as the penetration depth is much less than infinity in reality, particularly when losses are included.

As the effective length is also unknown (and not independent from ε_{eff}, or equivalently A), measurements from two samples were previously used to 'calibrate' the parameter retrieval by solving simultaneous equations for l_{eff} and A [31]. It was assumed initially that these values were not strong functions of the change in dielectric constant, enabling them to be used for all concentrations of sugar. The previous calculations [31] only included 16 measurements, whereas a total of 60 measurements were collected. Thus, the retrieved phantom permittivity values were re-calculated for this paper using the original calibration-based method and the expanded data-set; the second mode ($n = 2$) was used.

The original method is as follows. First, the median of all the measurements for each phantom was taken to find the frequency of operation. Second, the measured relative dielectric constant was taken at the frequency of interest. Finally, by employing the calibration procedure (using the 5% and 10% phantom measurements), l_{eff} and A were calculated as 0.4794 m and 0.9693, respectively. Once the unknowns were found, the phantom dielectric properties were retrieved by inserting the measured frequency into (1b) and (2a). The results are given in Table II. However, the gap between the measured and retrieved relative dielectric constant, termed the retrieval error, increased with decreasing phantom dielectric constant (increasing sugar concentration), as shown in Table II, indicating that the l_{eff} and A cannot be considered as constants with respect to the permittivity change. The dielectric properties (Table II) were calculated considering only the frequencies consecutively increasing while the phantom dielectric constant was decreasing. The retrieval of the dielectric constant, through (1b) and (2a), is highly dependant on the calibration; thus, there is a need to eliminate the calibration step. Note that the 5% and 10% sugar concentrations were used for calibrating the resonator, so the results are shown for 15% sugar concentration and above.

TABLE II
COMPARISON OF THE RETRIEVED AND MEASURED RELATIVE DIELECTRIC CONSTANT FOR THE PHANTOMS USING THE ORIGINAL METHOD

Parameter	Value			
Sugar / %	30.00	25.00	20.00	15.00
f_r / MHz	676.20	662.50	652.90	648.90
Retrieved ε_{p}	16.90	21.50	24.90	26.50
Measured ε_{p}	24.60	26.40	28.10	29.30
Error / %	31.40	18.50	11.20	9.78

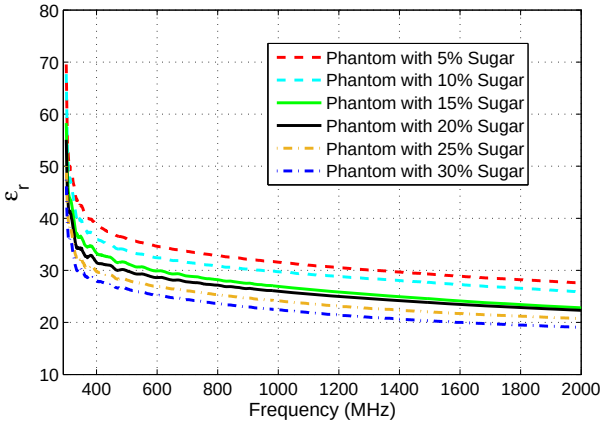

(a)

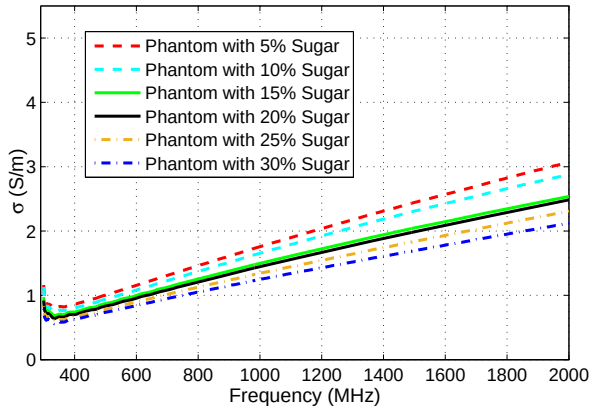

(b)

Fig. 4. Wide-band measurements of Phantoms with Agilent's open-ended coaxial probe: (a) permittivity measurements; (b) conductivity measurements.

C. Parameter Retrieval with Modified Analytical Method

The original method, reviewed in Section III-B, required a calibration procedure [31]. In the new approach, the calibration procedure was eliminated by utilizing the simulation results to predict the values of the unknown parameters, A and l_{eff}. In order to further decrease the retrieval error, A and l_{eff} were expressed as a function of frequency (f_r) and phantom dielectric constant (ε_{p}). To do so, twelve digital homogeneous phantoms, with different non-dispersive dielectric constants, were placed above the resonator in CST Microwave Studio and the simulated S parameter responses of the resonator recorded. The digital homogeneous phantoms were 30 mm thick, with the dielectric constants ranging from 15 to 40.5.

The operating frequencies of the resonator were determined for the different phantoms from the recorded S_{11} simulation results. The PSO algorithm was applied to the analytical formulation, as given by (1b)–(2), in order to find the corresponding A and l_{eff} for each simulation. The algorithm was given the resonant frequency and the phantom dielectric constant for each of the twelve CST simulations. The feasible solution space for A was the range 0.8 to 1, due to the construction of (2a) and considering the A value obtained from the calibration method. The solution space for l_{eff} was chosen to be from 0.224 m to 0.5 m. This range was chosen considering the physical length (0.224 m) of the resonator and the length of the resonator found using the calibration method (0.4794 m). Furthermore, the solution spaces for A and l_{eff} were successively reduced with each simulation, to ensure that they were both decreasing with increasing phantom permittivity. The fitness function for the algorithm was the phantom dielectric property retrieved from (2a). The threshold was set at 0.01%. To calculate the threshold, the absolute difference between the retrieved ε_{p} and given ε_{p} is calculated, the error determined by dividing the absolute difference by the given ε_{p}, and then the percentage calculated:

$$\text{Error}_{\%} = \frac{\left|\varepsilon_{\text{p}_g} - \varepsilon_{\text{p}_r}\right|}{\varepsilon_{\text{p}_g}} \cdot 100 \tag{3}$$

It is noted that experimentation with reducing the threshold resulted in a significant increase in the number of particles leaving the solution space; hence, the achieved solutions are highly likely to be the global solutions with the restricted solution space provided. We note that the PSO algorithm can settle to a local optimum if the problem is too complicated (e.g., if the problem has many parameters to optimize or if the function or design problem has many local minima) [33]–[36]. There are two traditional methods employed in the literature to overcome this issue: 1) using a linearly decreasing inertial weight, and 2) using an adequate number of particles. The first methodology helps the particle to be mostly pulled from the initial position at the beginning of the optimization. As the iteration progresses, the inertial weight decreases and the particle is mostly pulled by the personal and global best values. This approach prevents premature convergence and helps the particle converge towards the end of the iteration. It should be noted that inertial weight is only applicable for real PSO.

The second method helps by starting with a larger number of points in the search space, which eventually increases exploitation of the search space. Although these methods are effective for many problems, they may still fail to prevent premature convergence for complex design problems [35]. In our optimization algorithm, we adopted both of the above mentioned methods, such that our problem has only two variables with small search spaces, meaning particles can scatter to different positions in the search space, allowing them to explore the search space thoroughly.

Next, the filling factor and effective length were expressed as a function of resonant frequency and the relative dielectric constant of the phantom material using Multiple Linear Regression (MLR) and Multiple Non-linear Regression (MNLR) models [37, Ch. 12]. Different models of the relationships between frequency, phantom permittivity and filling factor or effective lengths were examined. Some were obviously worse than others. Here we show four forms for each parameter that were similar (in terms of goodness of fit, as measured by the correlation coefficient R), as examples. The equations for the models of l_{eff} are:

$$l_{\text{eff}_{(f_n,\varepsilon_{\text{p}})}} = a_1 + a_2\frac{c_0}{f_n} + a_3\frac{1}{\sqrt{\varepsilon_{\text{p}}}} \tag{4}$$

$$l_{\text{eff}_{(f_n,\varepsilon_{\text{p}})}} = a_1 + a_2\frac{c_0}{f_n} + a_3\frac{c_0^2}{f_n^2} + a_4\frac{1}{\sqrt{\varepsilon_{\text{p}}}} + a_5\frac{1}{\varepsilon_{\text{p}}} \tag{5}$$

$$l_{\text{eff}_{(f_n,\varepsilon_{\text{p}})}} = a_1 + a_2\frac{c_0}{f_n} + a_3\frac{c_0^2}{f_n^2} + a_4\frac{1}{\varepsilon_{\text{p}}} + a_5\frac{1}{\varepsilon_{\text{p}}^2} \tag{6}$$

$$l_{\text{eff}_{(f_n,\varepsilon_{\text{p}})}} = a_1 + a_2\sqrt{\frac{c_0}{f_n}} + a_3\frac{1}{\sqrt{\varepsilon_{\text{p}}}} \tag{7}$$

The equations for the models of A are:

$$A_{(f_n,\varepsilon_{\text{p}})} = b_1 + b_2\frac{{c_0}^2}{{f_n}^2} + b_3\frac{1}{\sqrt{\varepsilon_{\text{p}}}} \tag{8}$$

$$A_{(f_n,\varepsilon_{\text{p}})} = b_1 + b_2\frac{c_0}{f_n} + b_3\frac{{c_0}^2}{{f_n}^2} + b_4\frac{1}{\sqrt{\varepsilon_{\text{p}}}} + b_5\frac{1}{\varepsilon_{\text{p}}} \tag{9}$$

$$A_{(f_n,\varepsilon_{\text{p}})} = b_1 + b_2\sqrt{\frac{c_0}{f_n}} + b_3\frac{1}{\varepsilon_{\text{p}}} \tag{10}$$

$$A_{(f_n,\varepsilon_{\text{p}})} = b_1 + b_2\sqrt{\frac{c_0}{f_n}} + b_3\frac{1}{\sqrt{\varepsilon_{\text{p}}}} \tag{11}$$

The first two models for both parameters were based on physical considerations, particularly (1)–(2). The last two models are examples of models where different combinations were examined. The correlation of the regression lines with the PSO-derived data was used to determine which model should be used.

The right side of (1b) is equated to the right side of (2a), giving:

$$\left(\frac{nc_0}{l_{\text{eff}_{(f_n,\varepsilon_{\text{p}})}} f_n}\right)^2 = A_{(f_n,\varepsilon_{\text{p}})}\varepsilon_{\text{r}} + \left(1 - A_{(f_n,\varepsilon_{\text{p}})}\right)\varepsilon_{\text{p}} \tag{12}$$

Next, the functions for A and l_{eff} are inserted into (12), to be solved numerically for each phantom with the Newton-Raphson (NR) method. The initial guess for the NR method was chosen as 15 (for each phantom) and the solution space was constrained between 1 and 75 in order to prevent the method from finding negative and very high roots. These values were selected as the dielectric properties of human body tissues are located in this range.

Finally, the error in retrieved phantom dielectric constant (ε_{p_r}), compared with the given or measured relative dielectric constant (ε_{p_g}), is determined from (3).

IV. Results and Discussion

A. Permittivity retrieval using the spiral resonator

The simulated S_{11} response of the spiral resonator is shown in Fig. 5 for the different phantoms. The resonant frequency for each phantom was identified as being the frequency of the second notch, as this showed more variation with phantom

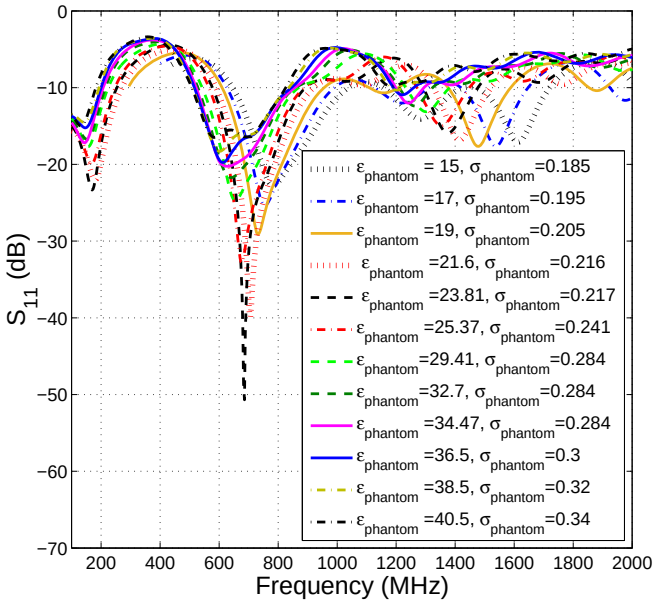

Fig. 5. Simulated performance of the spiral microstrip resonator with phantoms of varying permittivity, as determined by the impedance matching performance.

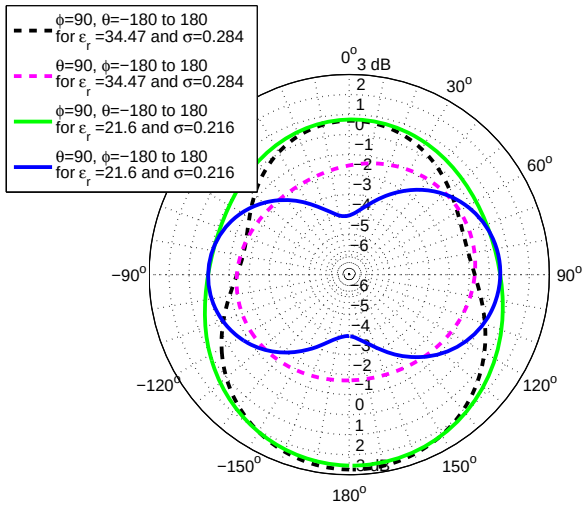

Fig. 6. Simulated radiation patterns of the digital phantoms with dielectric properties of ε_r=34.47 and $\sigma = 0.284$ s/m (dashed lines), and ε_r=21.6 and $\sigma = 0.216$ S/m (solid lines), which correspond to 5% and 30% sugar phantoms respectively.

permittivity than the first notch, and was usually somewhat narrower than the third notch. This corresponds to the $n = 2$ mode for the spiral resonator, as used in (1) and (12).

The radiation patterns of the simulations with those digital phantoms corresponding to 5% and 30% sugar phantoms, respectively, are shown in Fig. 6. Including more sugar decreases the relative permittivity of the phantom. Zero degrees in this plot corresponds to normal to the spiral and towards the phantom. It is clear that the gain level is marginally affected and the beam broadens slightly with increased sugar levels.

The simulated resonant frequencies and phantom permittivities were fed into the PSO algorithm. The PSO algorithm utilized the invisible boundary condition; that is, the particles could fly out of the defined solution space and were then simply assigned a bad fitness value. The solutions were reached using 50 particles within 13 to 87 iterations. The point estimations of the two unknowns were then used to fit a function to the obtained data set, given in Table IV, with the MNLR method. The regression coefficients of equations (4)–(8), and the corresponding R values (as a measure of the goodness of the proposed fitting function), are given in Table III. Note that the coefficients are calculated based on the data from the simulation response.

TABLE III
REGRESSION COEFFICIENTS AND R VALUES FOR THE CONSIDERED MULTIPLE NON-LINEAR REGRESSION EQUATIONS

l_{eff}	a_1	a_2	a_3	a_4	a_5	R
(4)	0.5859	−0.3565	−0.0416			0.9715
(5)	0.2080	1.6817	−2.1495	−1.1990	3.1980	0.9752
(6)	0.2753	1.0037	−1.4373	−0.9683	12.6386	0.9752
(7)	0.0807	−0.5514	−0.1117			0.9723
A	b_1	b_2	b_3	b_4	b_5	R
(8)	0.8642	−0.0222	1.9596			0.9654
(9)	1.5370	0.6975	−1.8092	−5.1694	11.9084	0.9939
(10)	0.9046	−0.0623	1.8796			0.9655
(11)	0.7712	−0.0052	0.8274			0.9526

Fig. 7(a) shows a graphical representation of the l_{eff} output for simulations from the PSO algorithm and the models fitted by MLR. From Fig 7(a), it can be seen that the functions are fairly similar; however, the function given in (5) has a numerically better fitting to the PSO output than that of (8), (6) and (7), as seen in Table III. Similarly, Fig 7(b) shows the functions fitted to the A coefficient PSO output; the function given in (9) has the better fitting. Hence, (5) and (9) were selected for use with the NR algorithm.

Both fitting functions—i.e., (5) and (9)—were analyzed to determine the reliability of the regression coefficients. Both A and l_{eff} were within the 95% confidence interval. The p value is much smaller than $\alpha = 0.05$. Thus, the outputs of the fitting function for the obtained data sets are deemed statistically significant.

Table IV shows a comparison of the retrieved phantom dielectric constant, the known dielectric constant given to the digital phantom during the simulation, and retrieval error, along with the operation frequencies. The retrieval error for all 12 digital phantoms is less than 3.34%. The sources of retrieval error are, first, the error resulting from the PSO algorithm's threshold and, second, the fitting functions for A and l_{eff}. The final error source is the solution space constraint for the NR model. The NR model suggests the following:

$$x_{\text{n+1}} = x_{\text{n}} - \frac{f_{(x_{\text{n}})}}{f'_{(x_{\text{n}})}} \tag{13}$$

Since the solution space is restricted in this case study, the left side of (13) should be replaced with $x_{\text{n+1}} + \triangle(n)$,

TABLE IV
DIELECTRIC CONSTANT RETRIEVAL FROM SIMULATION RESULTS, FOR PHANTOMS THAT ARE 33 MM BY 95 MM IN CROSS-SECTION AND 30 MM THICK ('NARROW LOAD').

Parameter	Value											
f_r / MHz	784.4	755.4	732.2	706.1	685.8	677.1	653.9	639.4	624.9	613.3	601.7	584.3
A	0.9972	0.9801	0.9551	0.9458	0.9377	0.9340	0.9283	0.9276	0.9192	0.9160	0.9094	0.9010
l_{eff} / m	0.4391	0.4386	0.4249	0.4246	0.4220	0.4188	0.4147	0.4134	0.4078	0.4057	0.3999	0.3963
Retrieved ε_{p}	14.9463	17.0723	19.0133	21.5704	23.9373	25.0842	28.6806	31.6105	34.6349	36.3650	38.5375	40.0611
Given ε_{p}	15	17	19	21.6	23.8	25.37	29.41	32.7	34.47	36.5	38.5	40.5
Error / %	0.3574	0.4258	0.0703	0.1370	0.5348	1.1262	2.4799	3.3318	0.4785	0.3698	0.0974	1.0836

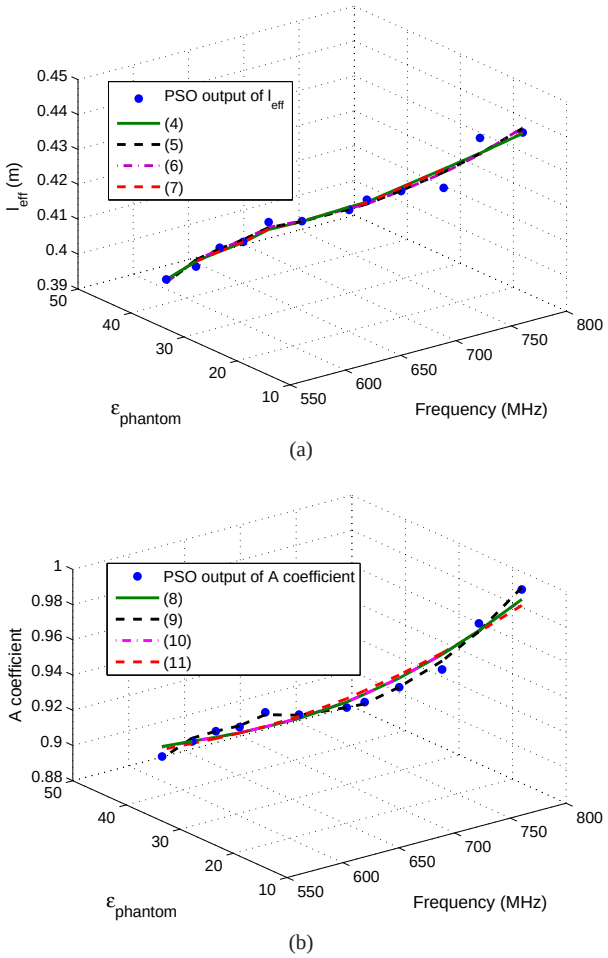

Fig. 7. Functions fit to PSO data with MLR for l_{eff} and A: (a) comparison between equations (4), (5), (6), and (7); (b) comparison between equations (8), (9), (10), and (11). The blue dots show the data obtained from the PSO algorithm.

with $\triangle(n)$ representing the error due to the feasible solution space constraint. The constraint directly affects the retrieved relative dielectric constant; however, without the restriction of the solution space, the NR method might give very high or low roots, meaning such a restriction is necessary.

Table V shows the comparison between the retrieved and measured dielectric properties. The measured ε_{p} values are the dielectric property measurements performed by using Agilent's open ended high temperature dielectric probe at the corresponding frequencies. Note that, as the measurements

TABLE V
COMPARISON OF THE RETRIEVED AND MEASURED RELATIVE DIELECTRIC CONSTANT FOR THE SOLID PHYSICAL PHANTOMS USING THE MNLR-BASED ANALYTIC FORMULATION

Parameter	Value					
Sugar / %	30	25	20	15	10	5
f_r / MHz	676.2	662.6	652.9	648.9	634.3	628.7
$\varepsilon_{\text{p}_{\text{Retrieved}}}$	25.2043	27.2273	28.8468	29.5938	33.2904	34.0235
$\varepsilon_{\text{p}_{\text{Measured}}}$	24.6240	26.4059	28.1296	29.3185	32.1132	34.3661
Error / %	2.3570	3.1109	2.5498	0.9391	3.6660	0.9967

are taken between 300 MHz to 2 GHz with sixteen hundred points, the resonant frequencies may not correspond to the measurement frequencies. In such cases, the closest frequency of the dielectric probe measurement is chosen as the reference dielectric property measurement. Note that the dielectric properties are a smooth function of the frequency; thus, such an approximation is valid and the error introduced is expected to be small in comparison to other error sources.

The error percentage is calculated using (3), which gives less than 3.67% for all measurements. The discrepancy between the retrieved and measured phantom dielectric properties can be partially attributed to measurement errors (i.e., in addition to the sources of retrieval error related to the retrieval method, discussed above). Two different measurement errors may have occurred: 1) measurement error due to the spiral resonator; and 2) measurement error due to the coaxial probe.

B. Measurement Error due to the Spiral Resonator

The differences between simulated and fabricated resonators (e.g., effect of the SMA connector and solder) are an obvious source of error in resonant frequency, as seen from Fig. 2. However, this type of error is relatively easy to minimize with advanced modeling techniques, so will not be discussed further here. In addition, this error is not as severe when the resonator is loaded with the phantoms, as shown by results discussed below.

During the simulations, the size and shape of the phantoms were considered ideal and homogeneous. However, the shape and condition of the phantom may not be ideal for the measurements. Thus, such imperfections can introduce measurement errors. From the simulations, we know that the thickness of the sample phantom affects the resonance of the spiral sensor. As the sample thickness increases, the effective permittivity increases; thus, the resonator starts to operate at

lower frequencies. The effect of thickness was investigated by simulating the spiral structure with five phantom samples having the thickness of 10 mm to 30 mm. The dielectric properties of the phantoms are kept constant ($\varepsilon_r = 32.7$ and $\sigma = 0.284$ S/m) and the size of the phantoms are 95 mm by 33 mm. The change in the return loss response is given in Fig. 8. From the simulation results, we conclude that the response of the resonator is affected by the phantom thickness for four samples, increasing the resonance response by around 17 MHz; however, the linearity changes with the 30 mm phantom.

To further understand the real effect of the load size on the response of the spiral resonator, it was simulated with two loads of different sizes. The phantoms were named wide and narrow loads and both had the same dielectric properties: $\varepsilon_r = 32.7$ and $\sigma = 0.284$ S/m. Note that the dielectric properties correspond to the 10% sugar concentration phantom. The surface dimensions of the wide load were 125 mm by 125 mm, and the dimensions of the narrow load were 95 mm by 33 mm (corresponding to the dimensions of the physical phantoms used in Section IV-A). Both phantoms had the same thickness of 30 mm. The resonator response was also measured with an equivalent wide load physical phantom. The wide load phantom was composed by following the recipe of oil-in-gelatine phantoms, that has been used to mimic the dielectric properties of biological tissues [38]. The wide load was a liquid phantom when first composed; it solidified over night at room temperature. To perform the measurement, the resonator was mounted at the bottom of a plastic container, facing upwards, with the container dimensions of 125 mm by 125 mm. The liquid wide load was poured into the container to a thickness of 30 mm and left overnight to solidify. The S-parameter response of the resonator was then collected.

After the measurements of the spiral resonator response were complete, the dielectric properties of the phantom were measured with Agilent's high temperature dielectric probe. Dielectric property measurements were collected at 10 points, twice from each point (including both top and bottom surfaces of the phantom) and averaged to obtain the properties given in Fig. 9. The measured dielectric properties at 600 MHz are $\varepsilon_r = 30.53$ and $\sigma = 0.5043$ S/m. The measurement set-up with the spiral structure is shown in Fig. 10. Note that all measurements were collected within 24 hours of the phantom composition. The comparison of the return loss responses for the wide and narrow loads is given in Fig. 11. Although there is a dielectric property discrepancy between the physical and digital phantoms, the simulated and the measured return loss for the wide load phantom agree well, with a 19.5 MHz discrepancy in resonant frequency. Similarly, the narrow load measurement and simulation also agree reasonably well, with a relatively small 13.7 MHz discrepancy observed between measured and simulated return loss responses. However, when the simulations for the narrow and wide loads were compared, we observed a 95.7 MHz discrepancy between the resonance frequencies, indicating that the phantom dimensions should be taken into account.

From the presented analysis, it is evident that the thickness and other dimensions of the phantoms have a significant effect

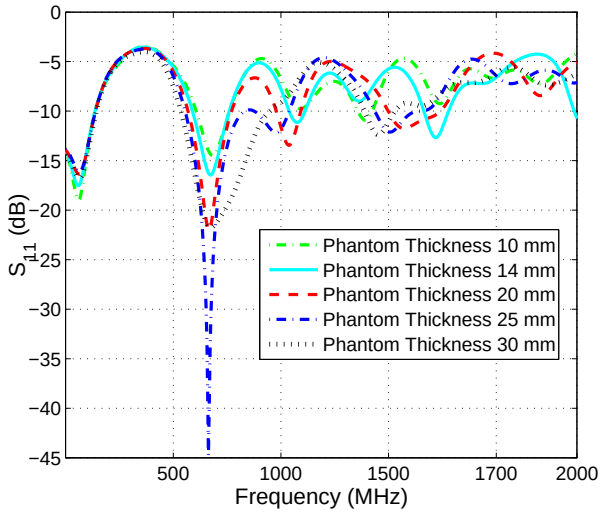

Fig. 8. Return loss response of the resonator with respect to the changes in the thickness of the phantoms.

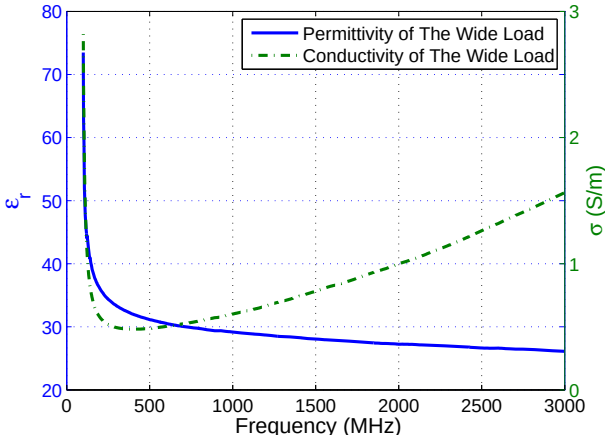

Fig. 9. Conductivity and permittivity measurements of the wide-load phantom.

on the return loss response of the resonator. Thus, differences in phantom shape and size result in retrieval errors. We can conclude that, for the intended application of non-invasive blood glucose monitoring, the sensor is subject-specific and could require some form of calibration as a result, particularly if absolute BGL measurements are desired. However, more information on this is required before any firm conclusions can be drawn.

C. Measurement Error due to the Coaxial Probe

The second error source is the dielectric property measurements performed with Agilent's open ended coaxial probe. The dielectric probe can pick up faulty measurements if the probe is not in good contact with the sample and the high temperature probe has a flange that prevents the experimenter from inspecting the instrument by eye, especially when opaque samples were used. Apart from the physical limitations, the probe itself may introduce measurement errors. The accuracy of the high temperature dielectric probe is given by [39]:

$$\hat{\varepsilon}'_{\mathrm{r}} = \varepsilon'_{\mathrm{r}} \mp \ 0.05 \ |\varepsilon^*_{\mathrm{r}}| \tag{14}$$

(a) (b)

Fig. 10. Measurement setup: (a) return loss measurement with wide load; and (b) resonator mounted in a container with the wide load phantom above.

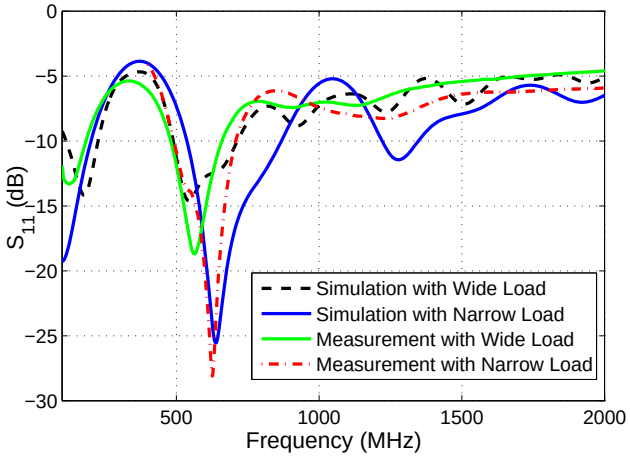

Fig. 11. Return loss response of the resonator with wide and narrow loads.

ε_r' is the relative dielectric constant and ε_r^* complex dielectric property of the sample. $\hat{\varepsilon}_r'$ is the estimate of the relative dielectric constant. In this study, the measured relative dielectric constant of the phantoms varies between 24 and 35 and the measured conductivity varies between 0.19 S/m and 0.4 S/m at the frequency of interest. Therefore, it is expected that the error in the phantom relative permittivity measurement (which is the reference for the spiral resonator measurements) is in the range of 1 to 1.7.

To examine the measurement errors that can be introduced by the coaxial probe, the dielectric property measurements given in Fig. 9 was analyzed. Considering the frequency of interest, the mean and standard deviation for 20 measurements taken from the same sample were calculated. The mean relative dielectric constant at 600 MHz is 30.5 and the standard deviation is 3.04. This implies a potential error of more than 10% for measured values outside one standard deviation, which could be a significant source of error when using the coaxial probe measurements as the reference for evaluating the performance of the spiral resonator and the models represented by (5) and (9).

D. Discussion

It has been demonstrated that it is possible to use numerical techniques to relate the phantom permittivity and resonant frequency of a microstrip spiral resonator with small error. The error sources have been investigated and a number of significant sources relate to the measurement of the reference data, giving further confidence that the error in the resonator and numerical method are acceptable.

It may be asked, what is the best resonator mode to use? There are two factors that must be considered: obtaining the necessary accuracy, and meeting regulatory requirements with regard to field exposure and heating for biological applications. Hence, the choice of resonator geometry and operating frequency must be made so that the field penetrates the sample (tissue) sufficiently, to ensure a reasonable averaging across the tissues and to ensure those tissues most responsive to glucose changes are included, whilst also meeting safety requirements. Having chosen the spiral geometry for reasons of compactness, the mode can be chosen to give the desired field pattern, and the spiral dimensions adjusted to achieve this mode at the desired frequency, to meet the required penetration and safety criteria.

It has been demonstrated that the dielectric properties of high water content tissues can be retrieved for narrow bands by employing an analytical equation. However, it is apparent that various error sources must be better understood and compensated for in a practical system. Moreover, the effect of the tissue thickness, shape, and reference dielectric property measurement is techniques have a significant effect on dielectric property reconstruction. For general dielectric samples, modification of the MNLR model to account for other factors may be possible. For blood glucose monitoring, the performance of a potential on-body resonator will be dependent on the tissue composition, age, gender, and body mass index of the patient. These issues may imply the need for periodic calibration using conventional bio-sensor monitoring techniques in a practical system; however, it may still be possible to significantly reduce the frequency of blood sampling required compared to existing solutions. Furthermore, *in vivo* experiments with a large enough representative sample population should provide sufficient data to allow the low error rate to be maintained, or even improved, particularly when further analysis of the error sources may help refine the analytical model and improve performance when applied to measured results.

It is worth noting that the value measured by commercial blood glucose monitors "*...should agree with a laboratory measurement within* $\pm 20\%$ *most of the time under normal conditions*" [10]. This relatively large margin of allowable error is a consequence of clinical considerations (i.e., considerations regarding whether clinical interventions are required), and can be understood in terms of the Clarke error grid [40] and similar constructs. Hence, the observed error from the numerical approach would appear to be well within this limit. Of course, our error is in retrieved permittivity, not blood glucose level, so a direct comparison is not intended. However, for a controlled experiment with no other factor affecting the permittivity, the likely error in detecting the change in sugar level (by mapping it to the dielectric constant) will not increase significantly from that of the error in the retrieved phantom permittivity. In addition, the concentrations of sugar used in this study are far from normal blood sugar levels. Refinement

of the model and resonator for a more restricted range are required, with evaluations of the sensitivity and repeatability of the measurements of particular interest. These findings may, therefore, form the basis for the development of an on-body resonator for dielectric property change monitoring that could have applications in non-invasive blood glucose monitoring or stroke detection.

V. Conclusions

Microstrip resonators have a number of advantages (e.g., compact, low-cost, planar/conformal), but their application to dielectric property measurements is complicated by the need to deal with an effective medium. Comparatively simple geometries, such as rectangular patches, can be analyzed to produce extraction equations. Such equations are not found in the literature for the spiral resonator, however, leading to the use of numerical techniques.

A microstrip spiral resonator was designed and fabricated for dielectric property retrieval of biological tissues. The resonator was tested with six physical phantoms, composed of flour, de-ionized water, and sugar. The amount of sugar in the physical phantoms was altered from 5% to 30% in 5% increments. The resonator was also simulated with twelve digital cuboid phantoms, with different relative dielectric constants, placed above the resonator and the S_{11} response of the resonator was recorded. The simulated return loss response of the transmission line was used to determine the resonant frequency for each phantom (for the mode $n = 2$), which was then used to determine the values of two coupled parameters, A, and l_{eff}. This was done by finding an optimal solution for the analytical formulation with the PSO algorithm for each simulation response. This approach provided insight on the behavior of the resonator when the physical phantoms were placed above.

The obtained simulated data was utilized to express A and l_{eff} as a function of frequency and the relative dielectric constant of the phantom. The functions for A and l_{eff} were written using an MNLR model. The retrieval of the relative dielectric constants of the phantoms was performed by inserting the operating frequency of the resonator obtained from the measurements. Retrieved dielectric properties were compared with the dielectric property measurements taken with Agilent's open-ended high temperature dielectric probe. The retrieval error was found to be less than 3.67% for all phantoms. The dielectric property retrieval algorithm was also applied to the obtained simulation results and the retrieval error was found to be less than 3.4% for all twelve digital phantoms. It is possible that tuning the PSO configuration, or using an alternative optimisation technique, could reduce this error further. The use of additional terms and parameters in the MNLR model is also likely to reduce this error.

One issue needing careful consideration and further work is how to separate the effect of the change in BGL from the effect from other physiological processes on the dielectric constant of the human body tissue. Similar studies will also be performed, therefore, examining the other factors that affect effective permittivity. In addition, the use of this technique for non-biological material characterization requires a reduction in the errors, perhaps through the expansion of the MNLP models used to include other parameters affecting A and l_{eff}. Finally, the application of this numerical approach to other types of resonator is another avenue for exploration.

References

[1] T. Yilmaz, R. Foster, and Y. Hao, "Detecting vital signs with wearable wireless sensors," *Sensors*, vol. 10, no. 12, pp. 10 837–10 862, 2010.

[2] Y. Hao and R. Foster, "Wireless body sensor networks for health-monitoring applications," *Physiological Measurement*, vol. 29, no. 11, p. R27, 2008.

[3] S. K. Vashist, "Continuous glucose monitoring systems: A review," *Diagnostics*, vol. 3, no. 4, pp. 385–412, 2013.

[4] Y. Hayashi, L. Livshits, A. Caduff, and Y. Feldman, "Dielectric spectroscopy study of specific glucose influence on human erythrocyte membranes," *Journal of Physics D: Applied Physics*, vol. 36, no. 4, pp. 369–374, 2003.

[5] T. A. Hillier, R. D. Abbott, and E. J. Barrett, "Hyponatremia: Evaluating the correction factor for hyperglycemia," *Am. J. Med.*, vol. 106, no. 4, pp. 399–403, 1999.

[6] E. Topsakal, T. Karacolak, and E. Moreland, "Glucose-dependent dielectric properties of blood plasma," in *The XXX General Assembly of the International Union of Radio Science*, Aug. 2011.

[7] B. Freer and J. Venkataraman, "Feasibility study for non-invasive blood glucose monitoring," in *IEEE Antennas and Propagation Society International Symposium (APSURSI)*, Jul. 2010, pp. 1–4.

[8] J. Venkataraman and B. Freer, "Feasibility of non-invasive blood glucose monitoring: In-vitro measurements and phantom models," in *IEEE Antennas and Propagation Society International Symposium (APSURSI)*, Jul. 2011, pp. 603–606.

[9] C. Hancock and S. Chaudhry, "A non-invasive monitoring system," in *European Microwave Conference*, Oct. 2007, pp. 313–316.

[10] B. R. Jean, E. C. Green, and M. J. McClung, "A microwave frequency sensor for non-invasive blood-glucose measurement," in *IEEESensors Applications Symposium (SAS)*, Feb. 2008, pp. 4–7.

[11] S. Pimentel, P. D. Agüero, A. J. Uriz, J. C. Bonadero, M. Liberatori, and J. C. neira Moreira, "Simulation of a non-invasive glucometer based on a microwave resonator sensor," *Journal of Physics: Conference Series*, vol. 477, no. 1, p. 012020, 2013, Paper presented at the 9th Argentinean Bioengineering Society Congress (SABI).

[12] M. Hofmann, G. Fischer, R. Weigel, and D. Kissinger, "Microwave-based noninvasive concentration measurements for biomedical applications," *IEEE Trans. Microw. Theory Techn.*, vol. 61, no. 5, pp. 2195–2204, May 2013.

[13] T. Yilmaz, R. Foster, and Y. Hao, "Broadband tissue mimicking phantoms and a patch resonator for evaluating noninvasive monitoring of blood glucose levels," *IEEE Trans. Antennas Propag.*, vol. 62, no. 6, pp. 3064–3075, Jun. 2014.

[14] D. M. Pozar, *Microwave Engineering*, 4th ed. John Wiley & Sons, Inc., Dec. 2011.

[15] K. Sarabandi and E. S. Li, "Microstrip ring resonator for soil moisture measurements," *IEEE Trans. Geosci. Remote Sens.*, vol. 35, no. 5, pp. 1223–1231, Sep. 1997.

[16] K. C. Gupta, R. Garg, I. Bahl, and P. Bhartia, *Microstrip Lines and Slotlines*, 2nd ed. Artech House, Inc., 1996.

[17] J. Svačina, "Analysis of multilayer microstrip lines by a conformal mapping method," *IEEE Trans. Microw. Theory Techn.*, vol. 40, no. 4, pp. 769–772, Apr. 1992.

[18] J. Svačina, "A simple quasi-static determination of basic parameters of multilayer microstrip and coplanar waveguide," *IEEE Microw. Guided Wave Lett.*, vol. 2, no. 10, pp. 385–387, Oct. 1992.

[19] J. T. Bernhard and C. J. Tousignant, "Resonant frequencies of rectangular microstrip antennas with flush and spaced dielectric superstrates," *IEEE Trans. Antennas Propag.*, vol. 47, no. 2, pp. 302–308, Feb. 1999.

[20] I. J. Bahl and S. S. Stuchly, "Analysis of a microstrip covered with a lossy dielectric," *IEEE Trans. Microw. Theory Techn.*, vol. MTT-28, no. 2, pp. 104–109, Feb. 1980.

[21] O. Isik and K. P. Esselle, "Design of monofilar and bifilar Archimedean spiral resonators for metamaterial applications," *IET Microw Antenna P*, vol. 3, no. 6, pp. 929–935, Sep. 2009.

[22] J. Kennedy and R. Eberhart, "Particle swarm optimization," in *IEEE International Conference on Neural Networks Proceedings*, vol. 4, Nov./Dec. 1995, pp. 1942–1948.

[23] T. Karacolak, A. Z. Hood, and E. Topsakal, "Design of a dual-band implantable antenna and development of skin mimicking gels for continuous glucose monitoring," *IEEE Trans. Microw. Theory Techn.*, vol. 56, no. 4, pp. 1001–1008, Apr. 2008.
[24] N. Jin and Y. Rahmat-Samii, "Parallel particle swarm optimization and finite-difference time-domain (PSO/FDTD) algorithm for multiband and wide-band patch antenna designs," *IEEE Trans. Antennas Propag.*, vol. 53, no. 11, pp. 3459–3468, Nov. 2005.
[25] J.-S. Chiang, Y.-K. Chou, W.-M. Hsu, and S.-H. Liao, "PSO and APSO for optimal antenna locations in indoor environment," in *International Conference on Intelligent Green Building and Smart Grid (IGBSG)*, Apr. 2014, pp. 1–4.
[26] K. Pereida and J. Guivant, "Hybrid Dijkstra-PSO algorithm for motion planning of non-holonomic multiple-trailer platforms in dense contexts," in *IEEE/ASME International Conference on Advanced Intelligent Mechatronics (AIM)*, Jul. 2013, pp. 13–18.
[27] M.-W. Li, W.-C. Hong, and H.-G. Kang, "Urban traffic flow forecasting using GaussSVR with cat mapping, cloud model and PSO hybrid algorithm," *Neurocomputing*, vol. 99, no. 0, pp. 230–240, 2013.
[28] R. Poli, J. Kennedy, and T. Blackwell, "Particle swarm optimization: An overview," *Swarm Intelligence*, vol. 1, no. 1, pp. 33–57, Jun. 2007.
[29] S. Seewattanapon, T. Wattakeekamthorn, T. Somwong, and P. Akkaraekthalin, "A microstrip folded resonator sensor for measurement of dielectric constant," in *5th International Conference on Electrical Engineering/Electronics, Computer, Telecommunications and Information Technology (ECTI-CON)* , vol. 1, May 2008, pp. 245–248.
[30] S. Seewattanapon and P. Akkaraekthalin, "A dual microstrip resonator for liquid dielectric constant measurement," in *Asia-Pacific Microwave Conference (APMC)*, Dec 2008, pp. 1–4.
[31] T. Yilmaz and Y. Hao, "Sensing of dielectric property alterations in biological tissues at microwave frequencies," in *Antennas and Propagation Conference (LAPC), 2011 Loughborough*, Nov. 2011, pp. 1–4.
[32] T. Yilmaz and Y. Hao, "Electrical property characterization of blood glucose for on-body sensors," in *Proceedings of the 5th European Conference on Antennas and Propagation (EUCAP)*, Apr. 2011, pp. 3659–3662.
[33] Y.-Y. Bai, S. Xiao, C. Liu, and B.-Z. Wang, "A hybrid IWO/PSO algorithm for pattern synthesis of conformal phased arrays," *IEEE Trans. Antennas Propag.*, vol. 61, no. 4, pp. 2328–2332, Apr. 2013.
[34] K. Saito and K. Suyama, "A local minimum stagnation avoidance in design of CSD coefficient FIR filters by adding Gaussian function," in *Asia-Pacific Signal and Information Processing Association Annual Summit and Conference (APSIPA)*, Oct. 2013, pp. 1–4.
[35] Y. Zhang, S. Wang, P. Phillips, and G. Ji, "Binary PSO with mutation operator for feature selection using decision tree applied to spam detection," *Knowledge-Based Systems*, vol. 64, no. 0, pp. 22–31, 2014.
[36] X. Yang, J. Yuan, J. Yuan, and H. Mao, "A modified particle swarm optimizer with dynamic adaptation," *Applied Mathematics and Computation*, vol. 189, no. 2, pp. 1205–1213, 2007.
[37] D. C. Montgomery and G. C. Runger, *Applied Statistics and Probability for Engineers*, 3rd ed. John Wiley and Sons, Inc., 2003.
[38] T. Yilmaz, R. Foster, and Y. Hao, "Patch resonator for non-invasive detection of dielectric property changes in biological tissues," in *IEEE Antennas and Propagation Society International Symposium (APSURSI)*, Jul. 2012.
[39] N. Wagner, M. Schwing, and A. Scheuermann, "Numerical 3-d FEM and experimental analysis of the open-ended coaxial line technique for microwave dielectric spectroscopy on soil," *IEEE Trans. Geosci. Remote Sens.*, vol. 52, no. 2, pp. 880–893, Feb 2014.
[40] W. L. Clarke, D. Cox, L. A. Gonder-Frederick, W. Carter, and S. L. Pohl, "Evaluating clinical accuracy of systems for self-monitoring of blood glucose," *Diabetes Care*, vol. 10, pp. 622–628, 1987.